

Analysis of thick plates by using a higher-order shear and normal deformable plate theory and MLPG method with radial basis functions

J.R. Xiao ^{a,*}, R.C. Batra ^d, D.F. Gilhooley ^{a,e,g}, J.W. Gillespie Jr. ^{a,b,c}, M.A. McCarthy ^{e,f,g}

^a Center for Composite Materials, University of Delaware, Newark, DE 19716, USA

^b Department of Materials Science and Engineering, University of Delaware, Newark, DE 19716, USA

^c Department of Civil and Structural Engineering, University of Delaware, Newark, DE 19716, USA

^d Department of Engineering Science and Mechanics, Virginia Polytechnic Institute and State University, Blacksburg, VA 24061, USA

^e Composites Research Centre, University of Limerick, Limerick, Ireland

^f Materials and Surface Science Institute, University of Limerick, Limerick, Ireland

^g Department of Mechanical & Aeronautical Engineering, University of Limerick, Limerick, Ireland

Received 28 November 2005; received in revised form 1 August 2006; accepted 1 August 2006

Abstract

Infinitesimal deformations of a homogeneous and isotropic thick elastic plate have been analyzed by using a meshless local Petrov–Galerkin (MLPG) method and a higher-order shear and normal deformable plate theory (HONSDPT). Radial basis functions (RBF) are employed for constructing trial solutions, while a spline function is used as the weight function over a local subdomain. The present method uses a number of randomly distributed nodes in the domain and is truly meshless. Two types of RBFs, i.e. multiquadrics (MQ) and thin plate splines (TPS), are employed and effects of their shape parameters on the quality of the computed solution are examined for deformations of thick plates under different boundary conditions. It is found that the present MLPG formulations give results very close to those obtained by other researchers. A benefit of using RBFs is that no special treatment is needed to impose the essential boundary conditions, which substantially reduces the computational cost.

© 2006 Elsevier B.V. All rights reserved.

Keywords: Higher-order shear and normal deformable plate theory; Thick plate; MLPG method; Radial basis function; Stress analysis

1. Introduction

Plates are widely used in a variety of applications; they may be homogeneous, laminated or functionally graded and their thickness depends upon the applications. The classical Kirchhoff thin plate theory, which ignores transverse shear effects, provides reasonable results for relatively thin plates, and suffices for computing the first few modes of bending vibrations. However, it may not give good values of higher modes of vibration for moderately thick

plates. In order to remedy this situation, a number of shear deformable plate theories have been developed. The simplest one is the first-order shear deformation plate theory such as the Reissner–Mindlin theory which assumes that the transverse shear strains are constant in the thickness direction and requires a shear correction factor to correct the discrepancy between the actual transverse shear stress distribution and that calculated using the plate theory. The value of the shear correction factor depends on geometric parameters, the loading and the boundary conditions. Second and higher-order shear deformation plate theories [1–4] use higher-order polynomials in the expansion of displacement components through the thickness of the plate and require no shear correction factor. Among them, the higher-order shear and normal deformable plate

* Corresponding author. Tel.: +1 302 8316109; fax: +1 302 8318525.
E-mail address: xiaoj@cmm.udel.edu (J.R. Xiao).

theory (HONSDPT) developed by Batra and his colleagues [3,5] accounts for both the transverse normal and the transverse shear deformations and uses Legendre polynomials as basis functions. Salient features of the theory include the satisfaction of natural boundary conditions prescribed on the top and the bottom surfaces of the plate, consideration of double forces without moments (i.e., equal and opposite tractions applied on the top and the bottom surfaces of a plate), and computations of the transverse normal and the transverse shear stresses from the plate equations rather than by integration through the thickness of the balance of linear momentum. The plate theory can accurately predict through-the-thickness modes of vibration which correspond to null lateral displacements or deflections. The plate theory was originally developed for piezoelectric plates. It has been used for studying free vibrations, and the propagation of plane waves in a thick anisotropic homogeneous plate [5], and static and dynamic deformations of isotropic homogeneous [6] and functionally graded thick plates [7].

Solutions of realistic engineering problems rely on appropriate numerical methods. Meshless methods have attracted increasing attention in the scientific community in recent years for seeking approximate solutions of initial-boundary-value and boundary-value problems governed by partial differential equations coupled with appropriate side conditions. These include the element-free Galerkin (EFG) method [8], the reproducing kernel particle method (RKPM) [9], hp-clouds [10], and the partition of unity method (PUM) [11]. However, all of these methods use a background mesh to numerically evaluate integrals appearing in the global weak formulation of the problem. The meshless local Petrov–Galerkin (MLPG) method developed by Atluri and his colleagues [12–15] is based on local weak rather than the global weak formulation of the problem, and does not require a background mesh for the evaluation of integrals in the weak formulation of the problem. Any non-element interpolation scheme such as the moving least square (MLS), or the PUM can be used to generate basis functions for the trial solution and, if desired, also for the test function. Similarly, Shepard functions can be used as basis functions for generating trial and test functions. Different test functions used in the MLPG method result in different MLPG schemes that have been labeled MLPG1–MLPG6 in [15].

Shepard functions and basis functions derived by the MLS approximation, the PUM, and the RKPM are rational functions. They lack the delta function property, which requires special techniques such as penalty parameters or Lagrange multipliers to satisfy essential boundary conditions. Static and transient infinitesimal deformations of thick elastic plates using Batra and Vidoli's plate theory [3] have been analyzed with the MLPG method and basis functions derived by the MLS approximation [7,8]. The matrix transformation technique was used to impose the essential boundary conditions, which considerably increased the computational cost. Recently radial basis

functions (RBFs) [16] have been used to solve partial differential equations [17–19] and in meshless methods [20–24]. The so derived shape functions possess the Kronecker delta function property, which allows the essential boundary conditions to be imposed easily. Furthermore, when RBFs are used in a local (compactly supported) rather than global interpolation scheme, such as in the MLPG method [22,23], the dense system matrices associated with the global interpolation scheme are avoided. The extended multi-quadrics, $g(r) = (r^2 + c^2)^\beta$, and thin plate splines (TPS) have been successfully employed in the MLPG method in [24] for the solution of two-dimensional stress analysis problems where the TPS was modified to $g(r) = r^\alpha \log r$ with α taken as a shape parameter. Here r is the distance between two points, and c and β are constants.

The analysis of plates using the compatible HONSDPT and meshless methods has been conducted in [6], where the MLS approximation was used for trial functions in both MLPG1 and MLPG5. In contrast to the two-dimensional solid mechanics problems [22], the MLPG5 in the HONSDPT has no advantage over other MLPGs because of non-vanishing domain integrals. The present paper aims to apply the above-mentioned RBFs with the MLPG method to the analysis of deformation of a thick plate using the compatible HOSNDPT. In the present study only MLPG1 is employed, and a fourth-order spline weight function is used as the test function. Two types of RBFs, MQ and TPS, are used as the trial function and the effect of their shape parameters on the accuracy of the approximate solutions is examined.

2. Brief review of the compatible HOSNDPT

A rectangular Cartesian coordinate system, shown in Fig. 1, is used to describe infinitesimal deformations of a rectangular elastic plate which occupies the region Ω defined by $0 \leq x \leq a$, $0 \leq y \leq b$ and $-t/2 \leq z \leq t/2$. The midsurface of the plate is denoted by S , and displacements of a point along the x , y and z axes by u , v , and w respectively. For through-the-thickness expansion of displacements, we use Legendre polynomials orthonormalized by

$$\int_{-t/2}^{t/2} L_i(z)L_j(z) dz = \delta_{ij}, \quad i, j = 0, 1, 2, \dots, \quad (1)$$

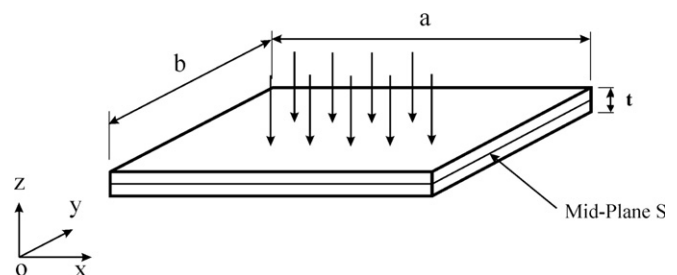


Fig. 1. Schematic sketch of the problem studied.

where δ_{ij} is the Kronecker delta. The first seven orthonormalized Legendre polynomials have the following expressions:

$$L_0(z) = \frac{1}{\sqrt{t}}, \quad L_1(z) = 2\sqrt{\frac{3z}{t}}, \quad L_2(z) = \frac{1}{2}\sqrt{\frac{5}{t}}\left[12\left(\frac{z}{t}\right)^2 - 1\right], \quad (2a)$$

$$L_3(z) = \sqrt{\frac{7}{t}}\left[-3\left(\frac{z}{t}\right) + 20\left(\frac{z}{t}\right)^3\right], \quad (2b)$$

$$L_4(z) = \frac{3}{\sqrt{t}}\left[\frac{3}{8} - 15\left(\frac{z}{t}\right)^2 + 70\left(\frac{z}{t}\right)^4\right],$$

$$L_5(z) = \sqrt{\frac{11}{t}}\left[\frac{15}{4}\left(\frac{z}{t}\right) - 70\left(\frac{z}{t}\right)^3 + 252\left(\frac{z}{t}\right)^5\right], \quad (2c)$$

$$L_6(z) = \sqrt{\frac{13}{t}}\left[-\frac{5}{16} + \frac{105}{4}\left(\frac{z}{t}\right)^2 - 315\left(\frac{z}{t}\right)^4 + 924\left(\frac{z}{t}\right)^6\right], \quad (2d)$$

$$L_7(z) = \sqrt{\frac{15}{t}}\left[-\frac{35}{8}\left(\frac{z}{t}\right) + \frac{315}{2}\left(\frac{z}{t}\right)^3 - 1386\left(\frac{z}{t}\right)^5 + 3432\left(\frac{z}{t}\right)^7\right]. \quad (2e)$$

We set

$$\mathbf{u} = \begin{Bmatrix} u(x, y, z) \\ v(x, y, z) \\ w(x, y, z) \end{Bmatrix} = \sum_{i=0}^K \begin{Bmatrix} u_i(x, y) \\ v_i(x, y) \\ w_i(x, y) \end{Bmatrix} L_i(z), \quad (3)$$

where K is the order of the plate theory. When $K \geq 2$, the plate theory is called higher order. It should be noted that u_i, v_i and w_i ($i = 0, 1, 2, \dots, K$) have the same dimensions. Recalling that $L'_i(z) = dL_i/dz$ is a polynomial of degree $(i - 1)$ in z , we write

$$L'_i(z) = \sum_{j=0}^K d_{ij} L_j(z), \quad (4)$$

where d_{ij} are constants. For $K = 7$,

$$d_{ij} = \begin{bmatrix} 0 & 0 & 0 & 0 & 0 & 0 & 0 & 0 \\ \sqrt{3} & 0 & 0 & 0 & 0 & 0 & 0 & 0 \\ 0 & \sqrt{15} & 0 & 0 & 0 & 0 & 0 & 0 \\ \sqrt{7} & 0 & \sqrt{35} & 0 & 0 & 0 & 0 & 0 \\ 0 & 3\sqrt{3} & 0 & 3\sqrt{7} & 0 & 0 & 0 & 0 \\ \sqrt{11} & 0 & \sqrt{55} & 0 & 3\sqrt{11} & 0 & 0 & 0 \\ 0 & \sqrt{39} & 0 & \sqrt{91} & 0 & \sqrt{143} & 0 & 0 \\ \sqrt{15} & 0 & 5\sqrt{3} & 0 & 3\sqrt{15} & 0 & \sqrt{195} & 0 \end{bmatrix}. \quad (5)$$

Note that elements in the first row and the last column of the $(K + 1) \times (K + 1)$ matrix d_{ij} are zeros. For infinitesimal deformations, the strains ε are given by

$$\varepsilon = \begin{Bmatrix} \varepsilon_{xx} \\ \varepsilon_{yy} \\ \varepsilon_{zz} \\ 2\varepsilon_{yz} \\ 2\varepsilon_{zx} \\ 2\varepsilon_{xy} \end{Bmatrix} = \sum_{i=0}^K \left\{ \begin{array}{l} \frac{\partial u_i(x, y)}{\partial x} \\ \frac{\partial v_i(x, y)}{\partial y} \\ \sum_{j=0}^K w_j(x, y) d_{ji} \\ \frac{\partial w_i(x, y)}{\partial y} + \sum_{j=0}^K v_j(x, y) d_{ji} \\ \frac{\partial w_i(x, y)}{\partial x} + \sum_{j=0}^K u_j(x, y) d_{ji} \\ \frac{\partial v_i(x, y)}{\partial x} + \frac{\partial u_i(x, y)}{\partial y} \end{array} \right\} L_i(z) \equiv \sum_{i=0}^K \{\eta_i\} L_i(z), \quad (6)$$

where for $i = 0, 1, 2, \dots, K$, η_i is a six-dimensional vector with components

$$\eta_{i(1)} = \partial u_i / \partial x, \quad \eta_{i(2)} = \partial v_i / \partial y, \quad \eta_{i(3)} = \sum_{j=0}^K d_{ji} w_j, \quad (7a)$$

$$\eta_{i(4)} = \partial w_i / \partial y + \sum_{j=0}^K v_j d_{ji}, \quad \eta_{i(5)} = \partial w_i / \partial x + \sum_{j=0}^K u_j d_{ji}, \quad (7b)$$

$$\eta_{i(6)} = \partial v_i / \partial x + \partial u_i / \partial y. \quad (7c)$$

The terms with d_{ij} couple K th order displacements with lower-order displacements. Using Hooke's law, stresses at a material point $\mathbf{x} = (x, y, z)$ are given by

$$\sigma = \{ \sigma_{xx} \quad \sigma_{yy} \quad \sigma_{zz} \quad \sigma_{yz} \quad \sigma_{zx} \quad \sigma_{xy} \}^T = \mathbf{D} \varepsilon, \quad (8)$$

where \mathbf{D} is the matrix of elastic constants. Substitution from Eqs. (6) and (7) into Eq. (8) gives stresses at a point (x, y, z) in terms of displacements and in-plane gradients of displacements of the point $(x, y, 0)$.

Let \tilde{u}, \tilde{v} and \tilde{w} be three linearly independent functions defined on the midsurface S given by $0 \leq x \leq a, 0 \leq y \leq b, z = 0$. Multiplying equations expressing the balance of linear momentum in the x -, y - and z -directions by \tilde{u}, \tilde{v} and \tilde{w} , respectively, adding the resulting equations, and using the divergence theorem, we obtain

$$\int_{\Omega} \tilde{\varepsilon}^T \sigma \, d\Omega - \int_{\partial\Omega} \tilde{u}^T \sigma n \, dS - \int_{\Omega} \tilde{u} f \, d\Omega = 0, \quad (9)$$

where \mathbf{n} is the unit outward normal on the boundary $\partial\Omega$, \mathbf{f} is the body force, and $\tilde{\varepsilon}$ is the strain vector obtained from Eq. (6). Substitution of (6) and (8) into (9) and integrating with respect to z from $-t/2$ to $t/2$ gives

$$\sum_{i=0}^K \left[\int_S \{\tilde{\eta}_i\}^T [D] \{\eta_i\} \, dS - \int_{\Gamma_u} \{\tilde{u}_i\}^T [n] [D] \{\eta_i\} \, d\Gamma - \int_{\Gamma_q} \{\tilde{u}_i\}^T \{\bar{q}_i\} \, d\Gamma - \int_S \{\tilde{u}_i\}^T \{\bar{f}_i\} \, dS - L_i(\pm t/2) \int_S \{\tilde{u}_i\}^T \{q^\pm\} \, dS \right] = 0, \quad (10)$$

where

$$\{\bar{q}_i\} = \int_{-1/2}^{1/2} L_i(z)\{q\} dz, \quad \{\bar{f}_i\} = \int_{-1/2}^{1/2} L_i(z)\{f\} dz \quad (11)$$

and $\{q^\pm\}$ is the traction on the top and the bottom surfaces of the plate, and Γ_u and Γ_q are disjoint parts of the boundary Γ of S , where displacements and surface tractions are prescribed, respectively, as \bar{u}_i and \bar{q}_i .

3. Interpolation using radial basis functions

Consider a continuous function $u(\mathbf{x})$ defined on the domain S containing a set of suitably distributed nodes. An interpolation of $u(\mathbf{x})$ in the neighborhood of the point \mathbf{x}_Q in Ω using RBFs and polynomial basis can be written as

$$u(\mathbf{x}, \mathbf{x}_Q) = \sum_{i=1}^n g_i(\mathbf{x})a_i(\mathbf{x}_Q) + \sum_{j=1}^m p_j(\mathbf{x})b_j(\mathbf{x}_Q), \quad (12)$$

$$\sum_{i=1}^n p_j(x_i, y_i)a_i = 0, \quad j = 1, 2, \dots, m, \quad (13)$$

where n is the number of nodes in the neighborhood of \mathbf{x}_Q , $g_i(\mathbf{x})$ is the RBF centered at the point \mathbf{x}_Q , $p_j(\mathbf{x})$ are monomials, m is the number of polynomial terms with $m \ll n$, and coefficients $a_i(\mathbf{x}_Q)$ and $b_j(\mathbf{x}_Q)$ are to be determined. The compact support of $g_i(\mathbf{x})$ is called the domain of influence of the point \mathbf{x}_Q .

Enforcing the interpolation to pass through all n scattered points within the influence domain gives n algebraic equations which coupled with m Eq. (13) can be solved for $a_i(\mathbf{x}_Q)$ and $b_j(\mathbf{x}_Q)$. Thus the trial solution in the neighborhood of the point \mathbf{x}_Q can be expressed as

$$u(\mathbf{x}) = \Phi(\mathbf{x})u^e, \quad (14)$$

where $u^e = [u_1, u_2, u_3, \dots, u_n]^T$, and the shape function $\Phi(\mathbf{x})$ is defined as

$$\Phi(\mathbf{x}) = [\phi_1(\mathbf{x}), \phi_2(\mathbf{x}), \phi_3(\mathbf{x}), \dots, \phi_k(\mathbf{x}), \dots, \phi_n(\mathbf{x})]. \quad (15)$$

Details of constructing shape functions and their derivatives can be found in [23].

Several RBFs are available; here, we use the following multiquadrics (MQ) and thin plate splines (TPS)

$$g_i(x, y) = (r_i^2 + c^2)^\beta \quad (\text{MQ}), \quad (16)$$

$$g_i(x, y) = (r_i)^\alpha \log r_i \quad (\text{TPS}), \quad (17)$$

where, β , c and α are shape parameters, and $r_i = [(x - x_i)^2 + (y - y_i)^2]^{1/2}$. The derivatives of MQ and TPS can be found in [24].

4. Implementation of the MLPG method for the compatible HONSDPT

4.1. Test functions for MLPG1

As mentioned above, we use the MLPG1 method in which the test function is taken as the weight function. That is,

$$\psi_J = W(\mathbf{x} - \mathbf{x}_J), \quad (18)$$

We use a fourth-order spline weight function defined as

$$W(\mathbf{x} - \mathbf{x}_J) = \begin{cases} 1 - 6\left(\frac{d_J}{r_s}\right)^2 + 8\left(\frac{d_J}{r_s}\right)^3 - 3\left(\frac{d_J}{r_s}\right)^4, & 0 \leq d_J \leq r_s, \\ 0 & d_J \geq r_s, \end{cases} \quad (19)$$

where $d_J = |\mathbf{x} - \mathbf{x}_J|$ and r_s is the size of the support of the weight function (same as the local subdomain). Thus the support of W is a circle of radius r_s centred at the node x_i .

4.2. Derivation of algebraic equations

The shape of subdomains can be chosen arbitrarily; however, subdomains are usually taken as circles or rectangles in two-dimensional problems; a circle is used here. Let $S_i \subset S$ be a smooth two-dimensional region associated with a node in S , $\Gamma_{ui} = \partial S_i \cap \Gamma_u$, $\Gamma_{qi} = \partial S_i \cap \Gamma_q$ and $\Gamma_{i0} = \partial S_i - \Gamma_{ui} - \Gamma_{qi}$. Let $\phi_1, \phi_2, \dots, \phi_N$ and $\psi_1, \psi_2, \dots, \psi_N$ be linearly independent functions defined on S_i . For a K th order plate theory there are $3(K + 1)$ unknowns at a point in S_i or S . We write these as a $3(K + 1)$ dimensional array and set

$$\{u(x, y)\} = \sum_{J=1}^N [\phi_J(x, y)]\{\delta_J\}, \quad (20)$$

$$\{\bar{u}(x, y)\} = \sum_{J=1}^N [\psi_J(x, y)]\{\tilde{\delta}_J\}, \quad (21)$$

where for each J , $\{\delta_J\}$ is a $3(K + 1)$ dimensional array and $[\phi_J]$ is a square matrix of $3(K + 1)$ rows and columns. Similarly $\{\tilde{\delta}_J\}$ is a $3(K + 1)$ dimensional array and $[\psi_J]$ is a square matrix of $3(K + 1)$ rows and columns. The shape functions ϕ_J are obtained using RBFs described above. The functions ψ_J are the weight functions, and the unknowns $\{\delta_J\}$ are the nodal displacements (similar to those in the finite element method). Substitution of (20) into (7) gives

$$\{\eta\} = \sum_{J=1}^N [B_J]\{\delta_J\}, \quad \{\tilde{\eta}\} = \sum_{J=1}^N [\tilde{B}_J]\{\tilde{\delta}_J\}, \quad (22)$$

where $\{\eta\}$ is a $6(K + 1)$ dimensional array and B_J is a $6(K + 1) \times 3(K + 1)$ matrix. The $6(K + 1)$ rows of B_J can be divided into $(K + 1)$ blocks of 6 rows each. The 6 rows of the i th block of B_J are given below.

$$\left[\begin{array}{ccc|ccc|ccc} \overbrace{0} & \overbrace{0} & \overbrace{0} & \overbrace{\partial\phi_J/\partial x} & \overbrace{0} & \overbrace{0} & \overbrace{0} & \overbrace{0} & \overbrace{0} \\ 0 & 0 & 0 & 0 & \partial\phi_J/\partial y & 0 & 0 & 0 & 0 \\ 0 & 0 & \phi_J d_{0i} & 0 & 0 & \phi_J d_{ii} & 0 & 0 & \phi_J d_{Ki} \\ 0 & \phi_J d_{0i} & 0 & 0 & \phi_J d_{ii} & \partial\phi_J/\partial y & 0 & \phi_J d_{Ki} & 0 \\ \phi_J d_{0i} & 0 & 0 & \phi_J d_{ii} & 0 & \partial\phi_J/\partial x & \phi_J d_{Ki} & 0 & 0 \\ 0 & 0 & 0 & \partial\phi_J/\partial y & \partial\phi_J/\partial x & 0 & 0 & 0 & 0 \end{array} \right], \quad (23)$$

where a repeated index is not summed. Elements of the matrix \tilde{B}_J are obtained from those of the matrix B_J by replacing ϕ_J with ψ_J .

Replacing the domain S of integration in Eq. (10) by S_i , substituting for $\{u\}$ and $\{\tilde{u}\}$ from Eqs. (20) and (21) and requiring that the resulting equation hold for all choices of $\{\tilde{\delta}\}$ we arrive at the following system of algebraic equations:

$$[K_{IJ}]\{\delta_J\} = \{F_I\}, \tag{24}$$

where

$$[K_{IJ}] = \int_{S_i} \left([\tilde{B}_I]^T [D] [B_J] \right) dS - \int_{\Gamma_{int}} \left([\psi_I]^T [n] [D] [B_J] \right) d\Gamma - \int_{\Gamma_{n0}} \left([\psi_I]^T [n] [D] [B_J] \right) d\Gamma, \tag{25a}$$

$$\{F_I\} = \int_{\Gamma_{qi}} [\psi_I]^T \{\bar{q}\} d\Gamma + \int_{S_i} [\psi_I]^T \{\bar{f}_i\} dS + L_i(\pm t/2) \int_{S_i} [\psi_I]^T \{q^\pm\} dS. \tag{25b}$$

Equations similar to Eq. (24) are obtained for each local subdomain S_i whose centre is at the node x_i . The Gauss quadrature rule of an appropriate order is employed to evaluate integrals over each local subdomain. For each quadrature point, interpolation is performed. Therefore for a node x_i there are two local domains: the test function domain (same as the local subdomain) for $\psi_J \neq 0$ (size r_s) and the interpolation domain for each Gauss point (size r_i). These two domains are independent of each other and are defined by $r_s = \alpha_s d_i$ and $r_i = \alpha_i d_i$, respectively. Here α_s and α_i are coefficients, and d_i is the distance from the node i to its nearest neighboring node.

5. Numerical examples

A number of problems have been solved to demonstrate the performance of the present method. For ease in comparison, results have been computed for a homogeneous and isotropic plate with $E = 2.068 \times 10^8$ Pa, $\nu = 0.3$, $a = 250$ mm, and unless otherwise specified, $K = 5$, which are the same as those used in [6]. Here E is Young’s modulus and ν Poisson’s ratio. A uniform distribution of nodes on the midsurface of plate is employed. The size of the subdomain is specified by setting $\alpha_s = 0.75$, and that of the interpolation domain by taking $\alpha_i = 4$. The following boundary conditions are imposed at a simply supported (S), a clamped (C), and a free (F) edge:

$$\begin{aligned} S: & \quad \sigma_{xx} = 0, \quad w = v = 0 \quad \text{on } x = 0, a; \\ & \quad \sigma_{yy} = 0, \quad u = w = 0 \quad \text{on } y = 0, b; \\ C: & \quad u = v = w = 0, \quad \text{on } x = 0, a; \quad y = 0, b; \\ F: & \quad \sigma_{xx} = \sigma_{xy} = \sigma_{xz} = 0 \quad \text{on } x = 0, a; \\ & \quad \sigma_{yy} = \sigma_{yx} = \sigma_{yz} = 0 \quad \text{on } y = 0, b. \end{aligned}$$

Recalling Eq. (3), it should be noted that $u = 0$ on $y = 0$ implies that $u_1 = u_2 = \dots = u_K = 0$, i.e., all components of the generalized displacements, including rotations, vanish at $y = 0$. The non-dimensional displacement $\bar{\mathbf{u}}$ is related to the dimensional displacement \mathbf{u} by

$$\bar{\mathbf{u}} = \frac{100Et^3}{12q_0a^4(1-\nu^2)} \mathbf{u}$$

where t is the plate thickness, and q_0 is the uniformly distributed traction on its top surface. Unless specified otherwise, 169 (13×13) uniformly distributed nodes were used to compute results presented and discussed below.

5.1. Radial basis functions and their shape parameters

The effect of shape parameters on the accuracy of the computed solution is first examined. The choice of shape parameters for MQ basis functions has received extensive attention. It seems that Wang and Liu [22] were the first to allow shape parameters of RBFs to be arbitrary real numbers and study their effect on the quality of the approximate solutions obtained by the EFG method. They pointed out that when β is close to 1, the accuracy of the numerical solution is higher ($\beta = 1.03$ was proposed as the optimal value). Xiao and McCarthy [23] have also studied the influence of the value of shape parameters of RBFs in the MLPG method, and found that when β is close to either 1 or 2, the computed solution is highly accurate and is much less sensitive to the value of the shape parameter c . Both 1.99 or 1.03 were suggested as the optimal values of β . They also found that the parameter c is sensitive to a characteristic nodal distance d , and established a linear relationship between the two. Good results were obtained for values of c between $5d$ and $7d$, and $c = 6d$ was recommended for two-dimensional solid mechanics problems. Rippl [24] and Wang [25] have given algorithms for adaptively selecting optimal values of the parameter c . In [26]

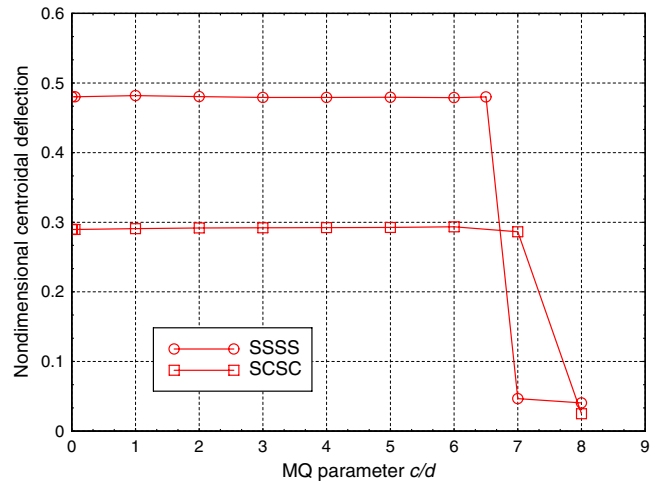


Fig. 2. Effect of the MQ shape parameter c on the centroidal deflection of two plates ($\beta = 1.99$) with different edge conditions.

Table 1
Non-dimensional centroidal deflection of a thick plate with $t/a = 0.2$ (IG = 5)

Method/reference	SSSS	SCSC	SFSF
MQ MLPG1	0.4792	0.2921	1.4358
TPS MLPG1	0.4803	0.2948	1.4430
MLS MLPG1	0.4798	0.2928	1.4362
MLS MLPG5	0.4793	0.2928	1.4368
Kant and Hinton	0.4900	0.3016	1.4496
Yuan and Miller	0.4905	0.3021	1.4542
Kant	0.4800	0.2930	1.4304
Kocak and Hassis	0.4782	0.2920	–
Lee et al.	0.4904	0.3021	1.4539

the optimal value of α was identified to be 4 when using the TPS radial basis functions in two-dimensional stress analysis problems. Furthermore, it was found that unlike for MQ, the TPS parameter is not sensitive to the characteristic nodal distance.

Here we investigate whether the optimal shape parameters established for two-dimensional solid mechanics problems hold for plate problems. For $\beta = 1.99$, the effect of the MQ shape parameter c is first studied for SSSS and SCSC plates. The computed non-dimensional centroidal deflections of the plate of aspect ratio $t/a = 0.2$, and the two sets of boundary conditions are presented in Fig. 2 for different

Table 2
Non-dimensional centroidal deflection of a square plate for different aspect ratios

Boundary conditions	t/a	MQ MLPG1	TPS MLPG1	MLS MLPG1	MLS MLPG5	Kocak & Hassis [4]	FEM [6]
SSSS	0.1	0.4223	0.4320	0.4220	0.4275	0.4200	0.4249
	0.2	0.4792	0.4803	0.4798	0.4793	0.4782	0.4803
	0.3	0.5698	0.5718	0.5717	0.5589		0.5710
	0.4	0.6952	0.7005	0.6967	0.6807		0.6952
	0.5	0.8508	0.8542	0.8511	0.8304		0.8487
CCCC	0.1	0.1457	0.1429	0.1468	0.1476	Srinivas and Rao [27] 0.1496	0.1486
	0.2	0.2089	0.2082	0.2112	0.2103	0.2134	0.2124
	0.3	0.3092	0.3090	0.3119	0.3064		0.3129
	0.4	0.4434	0.4434	0.4470	0.4408		0.4471
	0.5	0.6079	0.6079	0.6125	0.6050		0.6114

Table 3
Non-dimensional stress σ_{xx} at the center of the top surface of a thick square plate

	t/a	MQ MLPG1	TPS MLPG1	MLS MLPG1	MLS MLPG5	FEM [6]
SSSS	0.1	0.2890	0.2960	0.2887	0.2920	0.2900
	0.2	0.2996	0.3036	0.2984	0.3020	0.2976
	0.3	0.3141	0.3168	0.3129	0.3110	0.3099
	0.4	0.3392	0.3392	0.3333	0.3286	0.3283
	0.5	0.3750	0.3725	0.3640	0.3692	0.3568
CCCC	0.1	0.1430	0.1430	0.1432	0.1450	0.1440
	0.2	0.1596	0.1625	0.1617	0.1589	0.1613
	0.3	0.1899	0.1912	0.1895	0.1836	0.1877
	0.4	0.2304	0.2306	0.2274	0.2224	0.2235
	0.5	0.2825	0.2838	0.2877	0.2725	0.2725

Table 4
Non-dimensional stress resultant for a SCSC thick square plate

t/a	Point ($x/a, y/a$)	Stress resultant	MQ MLPG1	TPS MLPG1	MLS MLPG1	MLS MLPG5	Kant and Hinton [28]	Lee et al. [29]
0.1	(0.5, 0.5)	M_{xx}	0.0255	0.0256	0.0257	0.0251	0.0258	0.0258
	(0.5, 0.5)	M_{yy}	0.0330	0.0332	0.0333	0.0325	0.0332	0.0333
	(0.5, 0.0)	M_{yy}	0.0719	0.0632	0.0758	0.0726	0.0697	0.0680
	(1.0, 0.5)	Q_x	0.2484	0.1812	0.250	0.255	0.243	0.243
	(0.5, 0.0)	Q_y	0.5160	0.5040	0.4656	0.4884	0.5000	0.0500
0.2	(0.5, 0.5)	M_{xx}	0.0299	0.0301	0.0300	0.0298	0.0292	0.0292
	(0.5, 0.5)	M_{yy}	0.0338	0.0340	0.0341	0.0335	0.0330	0.0331
	(0.5, 0.0)	M_{yy}	0.0651	0.0584	0.0672	0.0641	0.0626	0.0627
	(1.0, 0.5)	Q_x	0.2520	0.2076	0.258	0.259	0.251	0.251
	(0.5, 0.0)	Q_y	0.5040	0.5640	0.4856	0.4820	0.4750	0.4750

Table 5
Non-dimensional stress resultant for a SFSF thick square plate

t/a	Point ($x/a, y/a$)	Stress resultant	MQ MLPG1	TPS MLPG1	MLS MLPG1	MLS MLPG5	Kant and Hinton [28]	Lee et al. [29]
0.1	(0.5, 0.5)	M_{xx}	0.1250	0.1250	0.1220	0.1230	0.1220	0.1220
	(0.5, 0.5)	M_{yy}	0.0258	0.0258	0.0261	0.0256	0.0256	0.0256
	(1.0, 0.5)	Q_x	0.4680	0.5840	0.4650	0.4660	0.4600	0.4600
0.2	(0.5, 0.5)	M_{xx}	0.1242	0.1236	0.1228	0.1224	0.1230	0.1230
	(0.5, 0.5)	M_{yy}	0.0262	0.0246	0.0245	0.0246	0.0237	0.0237
	(1.0, 0.5)	Q_x	0.4600	0.4920	0.4600	0.4640	0.4560	0.4560

values of the parameter c normalized by the nodal distance d . As for the two-dimensional solid mechanics problems [26], the computed deflections of the SSSS and the SCSC plates are essentially unchanged for c/d less than 6.5 and 7, respectively. However, for the plate problems, c/d can be very small (e.g., 1.0×10^{-8}) without any loss of accuracy. The computed values of stresses and force resultants show the same trend as those for deflections. We choose $c = 6d$ in the following work.

For the TPS shape parameter α , we computed results for SSSS, CCCC, SCSC, and SFSF plates with $\alpha = 2, 4$ and 6 , and observed only minor differences among the calculated deflections and stresses. Henceforth, we use $\alpha = 4$ as proposed in [26].

5.2. Comparison with published results

In order to study the performance of the present implementation, computed deflections of selected points of the midsurface of the plate for different edge conditions are compared, in Table 1, with those obtained by other investigators using either the HOSNDPT [6] or a first-order shear deformation theory [27–29]. Clearly, both the MQ and the TPS give results that are in excellent agreement with those of other researchers for each one of the three different boundary conditions. It should be noted that the present HOSNDPT does not need a shear correction factor as is used in the first-order shear deformation theory; also, the present meshless implementations are computationally more efficient than that with basis functions derived by the MLS approximation [6]. Table 2 compares the effect of the aspect ratio on the centroidal deflection of SSSS and CCCC plates; results with the finite element method (FEM) were obtained with the commercial code IDEAS by using 20-node brick elements [6], and the number of uniform elements in the x -, y - and z -directions were 40, 40, and 4, respectively. Again, the MLPG1 formulation with either the MQ or the TPS gives centroidal deflections that are very close to those obtained by other methods.

The calculated non-dimensional axial stress $\frac{\sigma_{xx}t^2}{q_0a^2}$ at the center of the top surface is compared with the published data in Table 3, and excellent agreement between the two is achieved for all thicknesses of the SSSS and CCCC plates. Stress resultants for plates with different boundary conditions are also compared in Tables 4 and 5, where

$$M_{xx} = \frac{1}{q_0a^2} \int_{-t/2}^{t/2} z\sigma_{xx} dz, \quad Q_x = \frac{1}{q_0a} \int_{-t/2}^{t/2} \sigma_{xz} dz$$

It can be seen that the MQ basis functions give excellent values of stress resultants at all locations. However, the accuracy of the computed stress resultants at boundary points using the TPS is not good as compared with that of the MQ and the MLS basis functions, though stress resultants calculated at the center point are in excellent agreement with those obtained with other methods [28,29].

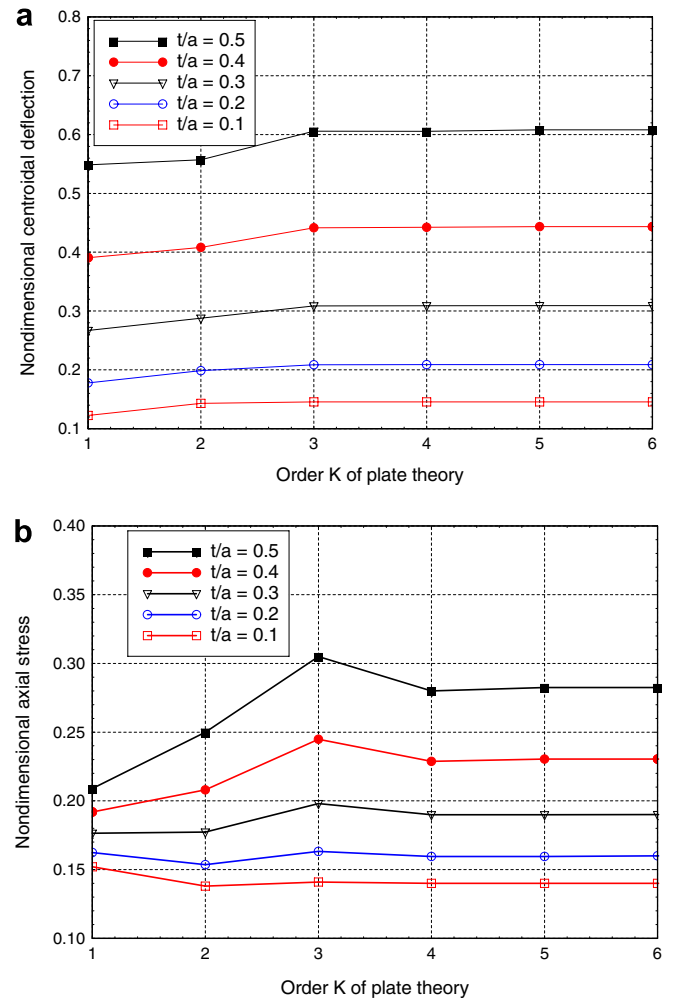


Fig. 3. Effect of the order K of the plate theory on (a) the centroidal deflection, and (b) the axial stress.

The number of Gauss points used in the above calculations is 36 (6×6). We now examine whether 36 Gauss points are sufficient for each one of the three types of boundary conditions stated above. For each case, virtually identical results were achieved when the number of Gauss points was increased from 36 (6×6) to 81 (9×9). However, fewer than 36 Gauss points may not give accurate results for plates with edges either clamped or traction free.

5.3. Order of plate theory

This section examines the effect of the order, K , of the plate theory on the computed results. For this purpose, we have plotted in Fig. 3, the non-dimensional centroidal deflection and the non-dimensional stresses at the center of the top surface of a CCCC plate for different values of K . It is evident that for a plate with $t/a > 0.1$ the lower order ($K < 3$) plate theory gives a smaller deflection than that obtained with the higher-order plate theory. One needs a plate theory of at least fourth-order to obtain reasonably good values of the axial stress. These conclusions agree

with those of [6] wherein basis functions derived by the MLS approximation were employed.

5.4. Effect of nodal placement

The convergence with an increase in the number of uniformly placed nodes on each side for the CCCC plate has been studied by computing results for six different nodal densities, namely 5×5 , 7×7 , 9×9 , 11×11 , 13×13 and 15×15 ; similar trends were seen for plates with other boundary conditions. Values of other parameters were $t/a = 0.1$, $K = 5$, $\alpha_s = 0.75$ and $\alpha_i = 4$. It can be seen from the results plotted in Fig. 4 that both the centroidal deflection and the axial stress at the center of the top surface computed with the two RBFs converge with an increase in the number of nodes; converged results are obtained with 169 nodes.

6. Conclusions

The meshless Local Petrov–Galerkin (MLPG) method with radial basis functions (RBFs) for the trial solution has been used to analyze deformations of an isotropic and homogeneous thick elastic plate. A higher-order shear and normal deformable plate theory (HONSDPT) developed by Batra and his colleagues has been employed. Two different RBFs have been examined and it has been found that the MQ basis functions give better accuracy than the TPS basis functions. Results with the MQ basis functions are sensitive to the choice of the value of the shape parameter divided by the distance between two adjacent nodes for a uniform placement of nodes. The accuracy of the TPS is comparable with that of the MQ for computing field variables at interior points of the midsurface but not for points close to the plate boundaries. However, results with the TPS basis functions were virtually independent of the choice of the parameter divided by the distance between two adjacent nodes. It was found that $\alpha = 2$ and 4 give equally good results for the present problems. The use of RBFs for the trial solution facilitates the imposition of essential boundary conditions which reduces the computational cost as compared to that when the MLS basis functions are employed. Results computed with the MLS basis functions depend on the value assigned to the penalty parameter used to enforce essential boundary conditions. Furthermore, the present work shows that the optimal values of shape parameters established for two-dimensional solid mechanics problems also hold for plate problems.

With the proposed RBF MLPG1 method, deformations of plates of different aspect ratios and boundary conditions have been analyzed. Computed deflections and stresses are found to match very well with those obtained with other methods including the three-dimensional analysis by the finite element method. Convergence studies with respect to the number of uniformly distributed nodes, and the order of the plate theory have been carried out. For $t/a \leq 0.1$, a third-order shear and normal deformable plate

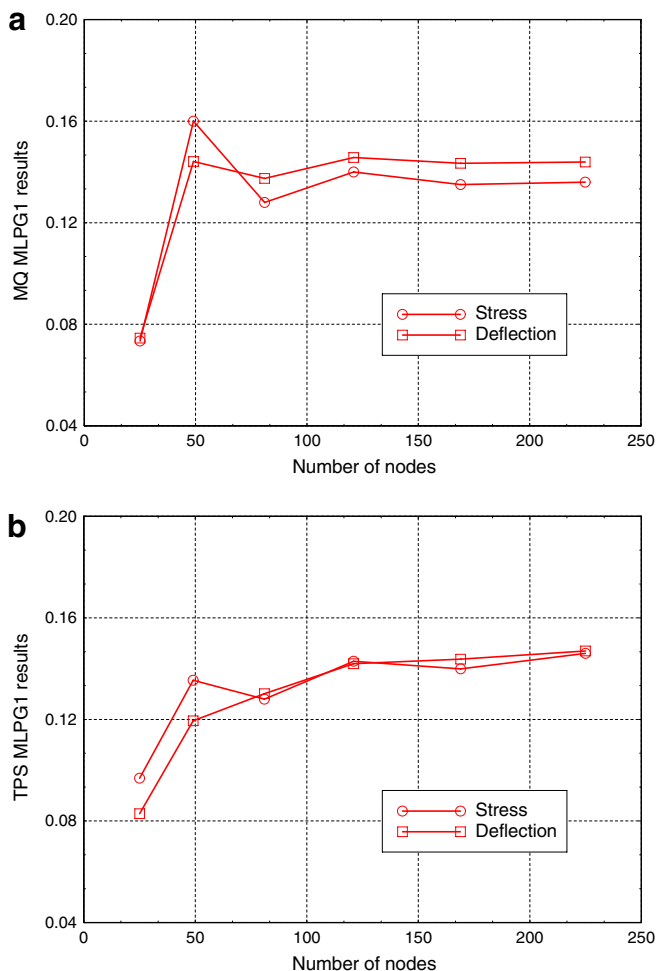


Fig. 4. For a CCCC plate, convergence of (a) the centroidal deflection, and (b) the axial stress at the center of plate's top surface. (a) MQ MLPG1 and (b) TPS MLPG1.

theory is adequate, but for $t/a > 0.1$, a fifth-order shear and normal deformable plate theory should be used.

Acknowledgements

D.F.G. acknowledges the support from the Irish Research Council for Science, Engineering and Technology Postgraduate Scholarship scheme to the University of Limerick, and the Internship from the University of Delaware Center for Composite Materials. R.C.B. acknowledges support from the ONR grants N00014-98-1-0300 and N0014-06-1-0567 to Virginia Polytechnic Institute and State University with Dr. Y.D.S. Rajapakse as the Program Manager.

References

- [1] K.H. Lo, R.M. Christensen, E.M. Wu, A higher-order theory of plate deformation, *J. Appl. Mech.* 44 (1997) 663–676.
- [2] N.D. Phan, J.N. Reddy, Analysis of laminated composite plates using a higher-order shear deformation theory, *Int. J. Numer. Methods Engrg.* 21 (1985) 2201–2219.
- [3] R.C. Batra, S. Vidoli, Higher-order piezoelectric plate theory derived from a three-dimensional variational principle, *AIAA J.* 40 (2002) 91–104.
- [4] S. Kocak, H. Hassis, A higher order shear deformable finite element for homogeneous plates, *Engrg. Struct.* 25 (2003) 131–139.
- [5] R.C. Batra, S. Vidoli, F. Vestroni, Plane wave solutions and modal analysis in higher order shear and normal deformable plate theories, *J. Sound Vib.* 257 (2004) 63–88.
- [6] L.F. Qian, R.C. Batra, L.M. Chen, Elastostatic deformations of a thick plate by using a higher-order shear and normal deformable plate theory and two meshless local Petrov–Galerkin (MLPG) methods, *Comput. Model. Engrg. Sci.* 4 (2003) 161–176.
- [7] L.F. Qian, R.C. Batra, L.M. Chen, Static and dynamic deformations of thick functionally graded elastic plate by using higher-order shear and normal deformable plate theory and meshless local Petrov–Galerkin method, *Composites: Part B* 35 (2004) 685–697.
- [8] T. Belytschko, Y.Y. Lu, L. Gu, Element-free Galerkin methods, *Int. J. Numer. Methods Engrg.* 37 (1994) 229–256.
- [9] W.K. Liu, S. Jun, Y. Zhang, Reproducing kernel particle methods, *Int. J. Numer. Methods Fluids* 20 (1995) 1081–1106.
- [10] C.A. Duarte, J.T. Oden, An h-p adaptive method using clouds, *Comput. Methods Appl. Mech. Engrg.* 139 (1996) 237–262.
- [11] I. Babuska, J. Melenk, The partition of unity method, *Int. J. Numer. Methods Engrg.* 40 (1997) 727–758.
- [12] S.N. Atluri, T. Zhu, A new meshless local Petrov–Galerkin (MLPG) approach in computational mechanics, *Comput. Mech.* 22 (1998) 117–127.
- [13] S.N. Atluri, H.G. Kim, J.Y. Cho, A critical assessment of the truly meshless local Petrov–Galerkin (MLPG), and local boundary integral equation (LBIE) methods, *Comput. Mech.* 24 (1999) 348–372.
- [14] S.N. Atluri, T. Zhu, The meshless local Petrov–Galerkin (MLPG) approach for solving problems in elasto-statics, *Comput. Mech.* 25 (2000) 169–179.
- [15] S.N. Atluri, S. Shen, *The Meshless Local Petrov–Galerkin (MLPG) Method*, Tech Science Press, 2002.
- [16] R.L. Hardy, Multiquadric equations of topography and other irregular surfaces, *J. Geophys. Res.* 76 (1971) 1905–1915.
- [17] E.J. Kansa, Multiquadrics – a scattered data approximation scheme with application to computational fluid-dynamics – I and II, *Comput. Math. Appl.* 19 (1990) 127–161.
- [18] M.A. Golberg, C.S. Chen, S.R. Karur, Improved multiquadric approximation for partial differential equations, *Engrg. Anal. Bound. Elem.* 18 (1996) 9–17.
- [19] G.E. Fasshauer, Solving partial differential equations by collocation with radial basis functions, in: A. Le M’ehaut’e, C. Rabut, L.L. Schumaker (Eds.), *Surface Fitting and Multiresolution Methods*, Vanderbilt University Press, Nashville, TN, 1997, pp. 131–138.
- [20] H. Wendland, Meshless Galerkin method using radial basis functions, *Math. Comput.* 68 (1999) 1521–1531.
- [21] G.R. Liu, Y.T. Gu, A local radial point interpolation method (LRPIM) for free vibration analysis of 2-D solids, *J. Sound Vib.* 246 (2001) 29–46.
- [22] J.G. Wang, G.R. Liu, On the optimal shape parameters of radial basis functions used for 2-D meshless methods, *Comput. Methods Appl. Mech. Engrg.* 191 (2002) 2611–2630.
- [23] J.R. Xiao, M.A. McCarthy, A local Heaviside weighted meshless method for two-dimensional solids using radial basis functions, *Comput. Mech.* 31 (2003) 301–315.
- [24] S. Rippa, An algorithm for selecting a good value for the parameter c in radial basis function interpolation, *Adv. Comput. Math.* 11 (1999) 193–210.
- [25] B.P. Wang, Parameter optimization in multiquadric response surface approximations, *Struct. Multidisci. Optim.* 26 (2004) 219–223.
- [26] J.R. Xiao, B.A. Gama, J.W. Gillespie Jr., E.J. Kansa, Meshless solutions of 2D contact problems by subdomain variational inequality and MLPG method with radial basis functions, *Engrg. Anal. Bound. Elem.* 29 (2005) 95–106.
- [27] S. Srinivas, A.K. Rao, Flexure of thick rectangular plates, *J. Appl. Mech.* 39 (1973) 298–299.
- [28] T. Kant, E. Hinton, Numerical analysis of rectangular Mindlin plates by segmentation method, Civil Engineering Department, Report: C/R365/80, University of Wales, Swansea, 1980.
- [29] K.H. Lee, G.T. Lim, C.M. Wang, Thick levy plate re-visited, *Int. J. Solids Struct.* 39 (2002) 127–144.